cedure and acid washing. In fact, almost no organic substances could be detected by gas chromatography–mass spectrometry after the vacuum heat treatment. These results indicate that the surface pretreatment of the sample is of great importance for improving the H_2 storage capacity of SWNTs, and systematic investigations of the pretreatment need to be carried out.

After adsorption equilibrium was achieved, the H_2 in the system was vented. The samples were then brought out and weighed, the results of which are shown in Table 1. There was a weight increase (0.5 to 1 weight %) for all three samples even after the stored H_2 was desorbed at room temperature. This implies that a certain amount of H_2 storage (21 to 25% of the total adsorbed H_2) could not be desorbed at ambient pressure and temperature. We tried heating these samples at 473 K and found that the weight increase disappeared, showing that essentially all the H_2 can be desorbed at elevated temperatures. This part of the residual H_2 may be related to chemical adsorption, which requires a higher energy for desorption. A few H_2 adsorption/desorption cycles were also carried out using the same experimental apparatus and parameters. The results show that after four cycles of adsorption/desorption, the H_2 uptake capacity of the SWNTs remained almost unchanged. The H_2 pressure has a great influence on its storage in the SWNTs. It was found that only a small amount of H_2 (less than 1 weight %) can be stored at pressures lower than 5 MPa, which is consistent with the results obtained at a cryogenic temperature of 80 K by Ye *et al.* (*2*).

The SWNT purity for sample 3 was estimated to be about 50 to 60 weight % from the results of thermogravimetric measurements and microscopic observations. It can then be expected that the H_2 adsorption capacity of pure SWNTs will likely be larger than 4.2 weight % even at room temperature under modestly high pressure. We argue that this relatively high H_2 adsorption capacity of our SWNTs may be related to their larger mean diameter. The results from our HRTEM observations show that our SWNTs have a mean diameter of 1.85 ± 0.05 nm, while typical SWNT diameters are in the range of about 1.2 to 1.4 nm (*6, 7*). From the Raman scattering spectrum of the sample, we found main peaks at 121 and 138 cm^{-1} in the low-frequency band, which was down-shifted from the corresponding Raman band for the SWNTs synthesized by the laser ablation method (*7*). These low-frequency peaks are considered to be related to the radial breathing mode (RBM) vibration of SWNTs, and the frequency of this radial mode is inversely proportional to the diameter of the SWNTs (*8*). The diameter of our SWNTs was determined by the Raman effect to be 1.85 and 1.62 nm, respectively, for the RBM peaks of 121 and 138 cm^{-1}, calculated from the equation of $\omega = 223.75/d$ given by Bandow *et al.* (*8*), where ω is the frequency of the RBM of SWNTs in units of centimeters^{-1} and d is the diameter of the SWNTs in nanometers. These results are therefore consistent with the HRTEM-observed diameter for our SWNTs. According to theoretical estimates, SWNTs with a larger mean diameter will allow greater H_2 storage (*1, 9*). The larger mean diameter of our SWNTs can be attributed to the addition of a sulfur-containing growth promoter (*10, 11*), which is a characteristic of our synthesis technique.

Although a H_2 adsorption capacity of 4.2 weight % was achieved at room temperature under modestly high pressure on the SWNTs synthesized by a semi-continuous hydrogen arc discharge method, further investigations are needed for this potentially high-capacity H_2 storage material.

References and Notes

1. A. C. Dillon *et al.*, *Nature* **386**, 377 (1997).
2. Y. Ye *et al.*, *Appl. Phys. Lett.* **74**, 2307 (1999).
3. A. Chambers, C. Park, R. T. K. Baker, N. M. Rodriguez, *J. Phys. Chem. B* **122**, 4253 (1998).
4. P. Chen, X. Wu, J. Lin, K. L. Tan, *Science* **285**, 91 (1999).
5. C. Liu *et al.*, *Carbon*, **37**, 1865 (1999).
6. C. Journet *et al.*, *Nature* **388**, 756 (1997).
7. A. M. Rao *et al.*, *Science* **275**, 187 (1997).
8. S. Bandow *et al.*, *Phys. Rev. Lett.* **80**, 3779 (1998).
9. S. D. M. Brown, G. Dresselhaus, M. S. Dresselhaus, *Mater. Res. Soc. Symp. Proc.* **497**, 157 (1998).
10. C. H. Kiang, W. A. Goddard III, R. Beyers, D. S. Bethune, *Carbon* **33**, 903 (1995).
11. H. M. Cheng *et al.*, *Chem. Phys. Lett.* **289**, 602 (1998).

12. We thank G. Dresselhaus, S. D. M. Brown, R. T. Yang, M. R. Black, and G. Su for their stimulating discussions. H.M.C. thanks National Natural Science Foundation of China for research grants 59872045 and 59672024, and the High-Tech Program of the Ministry of Science and Technology (MOST) of China. M.S.D. acknowledges support from NSF grant DMR 98-04734.

27 July 1999; accepted 4 October 1999

Polycationic Peptides from Diatom Biosilica That Direct Silica Nanosphere Formation

Nils Kröger,* Rainer Deutzmann, Manfred Sumper

Diatom cell walls are regarded as a paradigm for controlled production of nanostructured silica, but the mechanisms allowing biosilicification to proceed at ambient temperature at high rates have remained enigmatic. A set of polycationic peptides (called silaffins) isolated from diatom cell walls were shown to generate networks of silica nanospheres within seconds when added to a solution of silicic acid. Silaffins contain covalently modified lysine-lysine elements. The first lysine bears a polyamine consisting of 6 to 11 repeats of the *N*-methyl-propylamine unit. The second lysine was identified as ε-*N*,*N*-dimethyl-lysine. These modifications drastically influence the silica-precipitating activity of silaffins.

The chemical synthesis of silica-based materials like resins, molecular sieves, and catalysts requires extremes of temperature, pressure, and pH. In contrast, biosilicification proceeds at ambient temperatures and pressures, producing an amazing diversity of nanostructured frameworks (*1–4*). The silica cell wall of diatoms consists of two overlapping valves, and their structure is precisely controlled by the cell. During cell division a new valve is formed in minutes by controlled precipitation of silica within a specialized membrane vesicle called silica deposition vesicle (SDV) (*5*). Electron microscopic evidence indicates that the silica is initially deposited in the form of nanoscale spheres, suggesting the presence of components within the diatom cell that control silica sphere formation (*6*, *7*). However, the molecular structure of these components has remained elusive. It is well established that amorphous silica in diatom cell walls is intimately associated with organic substances that have been hypothesized to act as regulating molecules in biosilicification (*8–10*).

We examined the protein composition of cell walls from the diatom *Cylindrotheca fusiformis* (Fig. 1). Extraction of purified cell walls with EDTA led to the characterization of a Ca^{2+}-binding protein family called frustulins (*11*). Even after harsh extraction procedures with boiling SDS solutions the resulting silica preparation still contains tightly bound organic material that is recovered only after solubilizing silica with anhydrous hydrogen fluoride (HF). This HF-extractable material consists of two main protein fractions: a high molecular mass protein family, termed HEPs, that is localized at a specific substructure of the cell wall (*12*), and a low molecular mass fraction with apparent

Lehrstuhl Biochemie I, Universität Regensburg, 93053 Regensburg, Germany.

*To whom correspondence should be addressed. E-mail: nils.kroeger@vkl.uni-regensburg.de

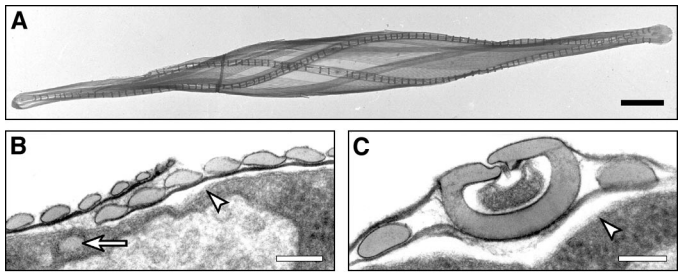

Fig. 1. Ultrastructure of *C. fusiformis* cell wall analyzed by transmission electron microscopy (TEM). (**A**) Isolated cell wall. Rows of parallel silica strips are running in a helical mode along the longitudinal axis of the cell. Bar: 2.5 μm. (**B** and **C**) Details of a *C. fusiformis* cell in cross section. The arrowheads indicate the position of the plasma membrane and point toward the extracellular space. Bars: 100 nm. (B) Lateral region. Each oval-shaped element represents a single silica strip of the cell wall in cross section. The arrow indicates a nascent silica strip within its SDV shortly before secretion. (C) Valve region. The ringlike structure and the two oval-shaped elements on either side are silicified cell wall elements.

masses ranging from 4 to 17 kD. Here we show that the latter (poly)peptides have affinity to silica; they are thus named silaffins. Silaffins appear to be the most abundant protein component within the HF extract of the cell wall, contributing about 50 μg per milligram of dry weight of EDTA-SDS–extracted cell wall material. Using Tricine-SDS polyacrylamide gel electrophoresis (PAGE) (*13*), silaffins fractionate into three components (Fig. 2A). NH_2-terminal amino acid sequencing indicates a high degree of homology between the 4-kD component, termed silaffin-1A [NH_2-terminus in single-letter amino acid symbols: SSXX′SGSYSG(S/Y)], and the 8-kD component, termed silaffin-1B (NH_2-terminus: SSXX′SGSYYSYGT). The fact that serine and tyrosine are simultaneously present in amino acid position 11 of silaffin-1A indicates that this component represents a mixture of almost identical polypeptides. Edman degradation of silaffin-1A and -1B, respectively, did not produce any signal at position 3 (X), whereas an unknown amino acid derivative was obtained at position 4 (X′). NH_2-terminal sequencing of silaffin-2 mainly produced unidentified phenylthiohydantoine (PTH) derivatives, indicating the presence of a different amino acid sequence with an even higher degree of posttranslational modification. Each of these silaffin species is able to precipitate silica within seconds when added to a freshly prepared solution of metastable silicic acid. The silicic acid solution without added silaffins did not form any precipitate and remained homogenous for at least a few hours. The amount of precipitated silica is proportional to the amount of silaffin applied (Fig. 2B). At any protein concentration, silaffins completely coprecipitate with the silica as long as silicic acid is present in excess. In the precipitate, the molar ratio silica/silaffin-1A is about 12 (*14*, *15*). As shown by scanning electron microscopy (SEM) (Fig. 2C), the silaffin-1A–induced precipitate is composed of a network of nearly spherical silica particles with diameters of 500 to 700 nm. Within the networks neighboring silica spheres are closely attached to each other or partly fused. When the unfractionated mixture of silaffins (Fig. 2A) was used for precipitation, aggregates of much smaller silica particles (diameters <50 nm) were obtained (Fig. 2 D).

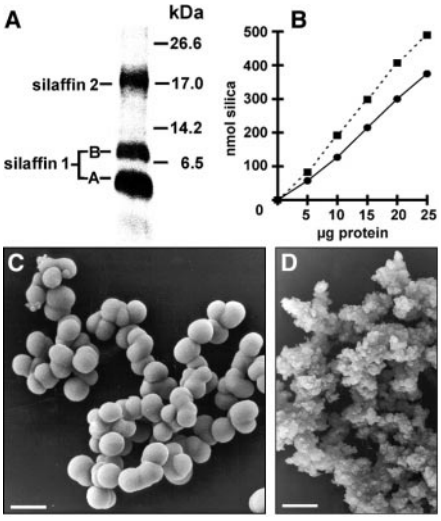

Fig. 2. Silica precipitation induced by silaffins (*14*). (**A**) Low molecular mass fraction of HF extract from *C. fusiformis* cell walls. The extract was subjected to Tricine–SDS-PAGE (*13*) and stained with Coomassie blue. (**B**) Correlation between silaffin concentration (*27*) and the amount of silica precipitated from a silicic acid solution. The dotted line represents the result obtained for the silaffin mixture; the solid line shows the result for pure silaffin-1A (*15*). (**C** and **D**) SEM micrographs of silica precipitated by silaffin-1A (C) and the mixture of silaffins (D). The diameter of silica particles is 500 to 700 nm (C) and <50 nm (D). The protein concentration was 5 mg/ml. Bar: 1 μm.

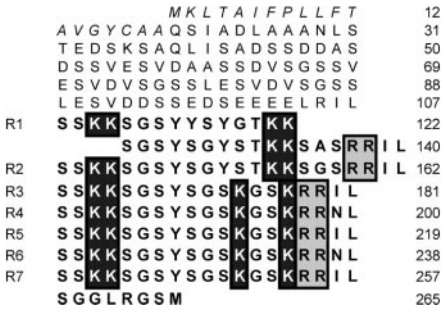

Fig. 3. Primary structure of sil1p. The signal peptide sequence is shown in italics, the highly acidic peptide sequence (residues 20 to 107) is depicted in regular type, and the mature part of the polypeptide (residues 108 to 271) is shown in bold. The repeats within the mature part bearing silaffin sequences are labeled R1 to R7 on the left margin. Arginine and lysine residues within silaffin sequences are highlighted. Abbreviations for the amino acid residues are as follows: A, Ala; C, Cys; D, Asp; E, Glu; F, Phe; G, Gly; I, Ile; K, Lys; L, Leu; M, Met; N, Asn; Q, Gln; R, Arg; S, Ser; T, Thr; V, Val; and Y, Tyr. The genomic sequence of *sil1* has been deposited in GenBank (accession number AF191634).

Using sequence information from the NH_2-terminus of silaffin-1B, we amplified by polymerase chain reaction (PCR) a corresponding cDNA fragment from a *C. fusiformis* cDNA library. This fragment was then used to screen a *C. fusiformis* genomic library, which led to the identification of a 795–base pair (bp) open reading frame, termed *sil1*, encoding a polypeptide (sil1p) of 265 amino acids (Fig. 3). Amino acid residues 1 to 19 represent a typical signal sequence followed by a peptide sequence (residues 20 to 107) highly enriched in acidic amino acid residues. The remaining COOH-terminal part of sil1p has a striking repetitive structure. It is composed of seven highly homologous repeating units (R1 to R7) containing 33 (R1), 22 (R2), and 19 (R3 to R7) amino acids, respectively. Basic amino acid residues predominate throughout this part of sil1p, particularly Lys-Lys and Arg-Arg clusters, which are spaced in a highly regular manner. In between these clusters, the hydroxy-amino acids serine and tyrosine predominate. The NH_2-terminal sequence of silaffin-1B exactly matches amino acids 108 to 120 of repeat unit R1, with both X and X′ representing lysine residues. Also, the NH_2-terminal sequences of silaffin-1A are contained within sil1p, being identical to the first 11 amino acids of each of the repeats R2 to R7, with X and X′ again representing lysine residues. Thus, comparison of sil1p sequence with the NH_2-terminal sequences of silaffin-1A and -1B led to the following conclusions. First, silaffin-1A and -1B originate from endoproteolytic processing of sil1p. This has been further confirmed by experiments described below. Second, the unidentified amino acid residues X and X′ in the NH_2-terminal sequences of silaffin-1A and -1B represent posttranslationally modified lysine residues.

To elucidate these modifications, we again subjected silaffin-1A to Edman degradation. The unknown lysine derivative liberated in cycle 4 (denoted X′) was then analyzed by electrospray ionization mass spectrometry (ESI-MS). A single peak of mass $(m + H)^+ = 292$ was detected. This mass exactly matches the value calculated for the PTH derivative of ε-*N*,*N*-dimethyl-lysine. Collision-induced fragmentation of this compound by tandem mass spectrometry (MS/MS) confirmed this conclusion, as the same fragment ion pattern was obtained when compared with authentic ε-*N*,*N*-

dimethyl-lysine (*16*). In contrast, no lysine derivative was detected in cycle 3 (denoted X) during Edman degradation of silaffin-1A. Therefore, a different approach was selected to identify this lysine derivative. Chymotryptic peptides derived from silaffin-1A were fractionated by reversed-phase high-pressure liquid chromatography (HPLC), which allowed the isolation of six peptides eluting at about 12% acetonitrile (*16*). All six peptides had the amino acid sequence SSXX′SGSY but different molecular masses. These masses differed by multiples of 71, indicating the presence of a repeated unit oligomer attached to these peptides.

Complete acid hydrolysis of silaffin-1A (6 N HCl at 110°C for 16 hours) did not hydrolyze the oligomeric structure. ESI-MS of the products of acid hydrolysis detected a series of singly charged ion masses that differed again by multiples of 71 (Fig. 4A). The values exactly matched the $(m + H)^+$ ion masses obtained by 5 to 11 repeats of a 71-dalton unit linked covalently to a lysine residue. The resistance of this oligomer to acid hydrolysis indicated a lysine-*N*-alkyl linkage. ^{1}H-Nuclear magnetic resonance (NMR) spectroscopy in D_2O produced a singlet resonance at 2.4 parts per million as well as a multiplet resonance at 2.65 ppm, indicating the presence of both N-CH_3 and N-CH_2-alkyl elements within the oligomer. A repeated *N*-methyl-propylamine unit attached to the ε-amino group of the lysine at position 3 of the chymotryptic peptides would explain both the NMR and the mass spectrometric data. Final proof for this structure was obtained by MS/MS analysis of the $(m + H)^+ = 573$ ion (six repeats of the unit element) of the acid hydrolysate (Fig. 4A). Fragmentation yields two series of subfragments with masses differing again by 71 daltons (Fig. 4B), confirming the proposed polyamine structure (Fig. 4C). Taking into account the masses of these lysine modifications allows the correct prediction of the experimentally determined masses of the chymotryptic peptides (see above; Fig. 4D).

Reversed-phase HPLC combined with ESI-MS and NH_2-terminal sequencing demonstrates that silaffin-1A is a mixture of peptide isoforms with molecular masses ranging from 2500 to 3500 daltons. These peptide isoforms represent the individual, covalently modified repeat units R2 to R7 of si/1p (Fig. 3). We have previously found that certain peptides terminating with the sequence motifs RHL or RQL become cleaved off from diatom cell wall proteins in vivo, suggesting that these motifs serve as recognition sites for a specific endopeptidase (*17*). Very similar motifs (RIL and RNL) terminate individual repeat stretches of the *sil1* gene product and thus may be responsible for the generation of silaffin-1A and -1B by endoproteolysis of the precursor polypeptide.

Evidence has been presented that silica formation in diatoms takes place in an acidic environment (*18*). To investigate the effect of the lysine modifications on silaffin function, we compared the silica precipitation activities of silaffin-1A and synthetic peptide pR5 at different pH values. Synthetic peptide pR5 corresponds to the amino acid sequence of repeat R5 of the silaffin precursor polypeptide (Fig. 3) and lacks any posttranslational modifications. pR5 has no silica precipitation activity below pH 7, whereas silaffin-1A activity is maximal around pH 5 and persists down to pH 4 (Fig. 5), showing that the lysine modifications present in silaffin-1A are required for silica-precipitating activity under physiological pH conditions.

The inorganic chemistry of silicic acid polycondensation ultimately leading to silica has been studied in detail (*19*). This complex process includes formation of colloidal silica (sol), transition to a gel, flocculation, and sintering. The rate of silica deposition found in biomineralization processes has been estimated to be about 10^6 times higher than abiotic silica formation from silicic acid (*7*). Therefore, the assumption was made that silica precipitation within the SDV involves flocculation of colloidal silica particles substantially greater in size than silicic acid monomers (*7*). Electron microscopic observations have indeed shown nanoscale silica spheres in nascent diatom cell walls (*20*–*22*). Our results demonstrate the in vitro formation of silica nanospheres within seconds in the presence of silaffins, producing a composite material rather than pure silica. Given the tight association of silaffins with diatom biosilica in vivo, it is reasonable to assume that silaffin-silica composites may be involved in

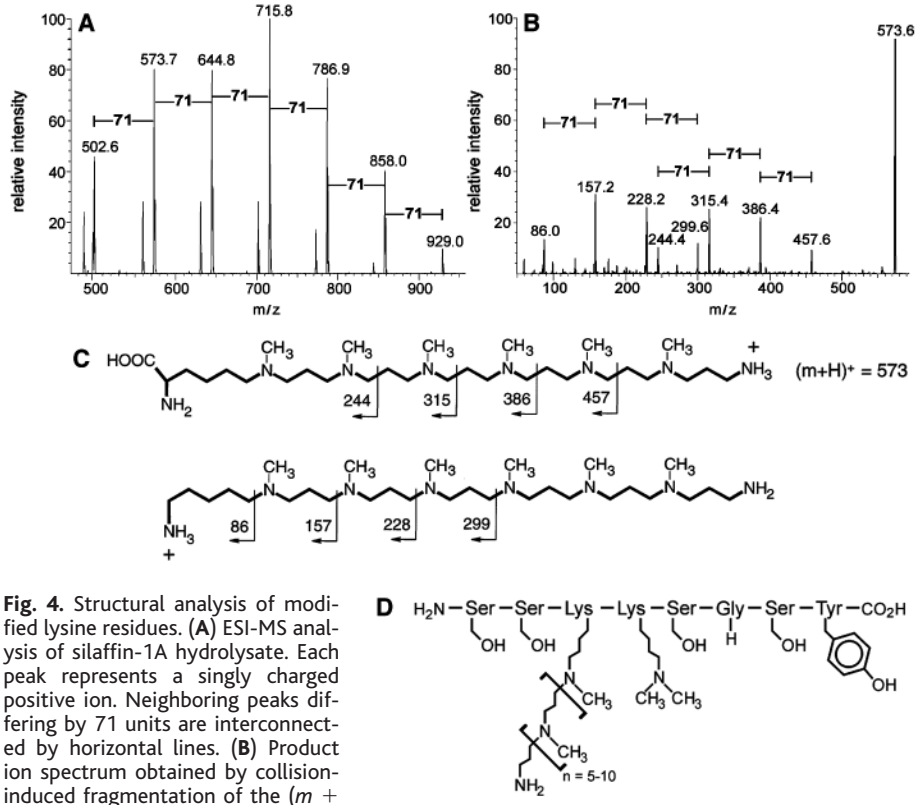

Fig. 4. Structural analysis of modified lysine residues. (**A**) ESI-MS analysis of silaffin-1A hydrolysate. Each peak represents a singly charged positive ion. Neighboring peaks differing by 71 units are interconnected by horizontal lines. (**B**) Product ion spectrum obtained by collision-induced fragmentation of the $(m + H)^+ = 573$ ion. Two series of ions (series 1: *m/z* 86, 157, 228, 299; series 2: *m/z* 244, 315, 386, 457; *m/z*: mass/ionic charge ratio) were detected. Within each series ion masses of neighboring peaks differ by 71 daltons (horizontal lines). (**C**) Proposed schematic structure of the $(m + H)^+ = 573$ ion. The molecule shown below the $(m + H)^+ = 573$ ion represents the decarboxylated derivative that gives rise to ion series 2 (B). Cleavage positions that lead to the observed fragment ions are depicted by rectangular arrows, and the corresponding masses are indicated above the arrowheads. (**D**) Schematic chemical structure of chymotryptic peptide SSXX′SGSY. The peptide backbone is indicated as three-letter amino acid symbols connected by horizontal lines. The structures of the side chains are shown below the respective amino acid symbol.

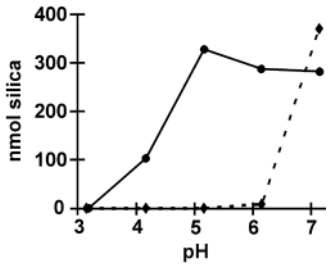

Fig. 5. pH dependence of peptide-induced silica precipitation. The solid line shows the result for silaffin-1A; the dotted line represents the result for synthetic peptide pR5. At each pH value, the amount of respective peptide applied was 28 nmol (*28*).

morphogenesis of the diatom cell wall. A completely different type of protein, a member of the papain family of proteolytic enzymes, was recently shown to be associated with silica spicules of a marine sponge (*23*). This protein catalyzes in vitro hydrolysis of silicon ethoxides (*24*) and thus may be involved in releasing silicic acid from a putative precursor molecule in vivo. In contrast, silaffins are ideally adapted to promote silicic acid polycondensation and precipitation of biogenic silica. First, as pointed out by Iler (*19*), possible candidates for flocculating agents involved in silica precipitation are cationic polymers and hydrogen-bonding polymers. Exactly these structural elements are present in silaffins, which are polycationic molecules containing a high proportion of hydroxyamino acids (predominantly serine) and are thus ideally suited for ionic and hydrogen-bonding interactions with the surface of silica particles. Second, silaffins are covalently modified by the oligo-*N*-methyl-propylamine unit that chemically resembles the polyamine structures found to catalyze silicic acid polymerization (*25*) and to promote silica flocculation (*26*). The modifications strongly increase the cationic charge of silaffins and were shown to be essential for silica formation at acidic pH values. Diatom SDVs have been shown to be acidic compartments (*18*), and therefore the polyamine structure is indispensable for silaffins to exert silica precipitation activity at the pH conditions within the SDV lumen. To our knowledge, the oligo-*N*-methyl-propylamine modification has not yet been found in any other biological system. Further analysis of the role of silaffins in nanofabrication of diatom cell walls might offer biomimetic approaches for the synthesis of siloxane-based materials.

References and Notes

1. S. Mann, *Nature* **365**, 499 (1993).
2. S. Oliver, A. Kupermann, N. Coombs, A. Lough, G. A. Ozin, *Nature* **378**, 47 (1995).
3. S. Mann and G. Ozin, *Nature* **382**, 313 (1996).
4. S. Mann, J. Webb, R. J. P. Williams, Eds., *Biomineralization: Chemical and Biochemical Perspectives* (VCH, Weinheim, Germany, 1989).
5. J. Pickett-Heaps, A. M. M. Schmid, L. A. Edgar, in *Progress in Phycological Research*, F. E. Round and D. J. Chapman, Eds. (Biopress, Bristol, UK, 1990), vol. 7, pp. 1–169.
6. B. E. Volcani, in *Silicon and Siliceous Structures in Biological Systems*, T. L. Simpson and B. E. Volcani, Eds. (Springer, New York, 1981), pp. 157–200.
7. R. Gordon and R. W. Drum, *Int. Rev. Cytol.* **150**, 243 (1994).
8. T. Nakajima and B. E. Volcani, *Science* **164**, 1400 (1969).
9. R. Hecky, K. Mopper, P. Kilham, T. Degens, *Mar. Biol.* **19**, 323 (1973).
10. D. Swift and A. Wheeler, *J. Phycol.* **28**, 202 (1992).
11. N. Kröger, C. Bergsdorf, M. Sumper, *EMBO J.* **13**, 4676 (1994).
12. N. Kröger, G. Lehmann, R. Rachel, M. Sumper, *Eur. J. Biochem.* **250**, 99 (1997).
13. H. Schägger and G. von Jagow, *Anal. Biochem.* **166**, 368 (1987).
14. Silica precipitation assay. A solution of orthosilicic acid was freshly prepared by dissolving tetramethylorthosilicate ester in 1 mM HCl to a final concentration of 1 M. Proteins to be tested for silica precipitation activity were dissolved in 100 mM sodium phosphate–citrate (buffered to the appropriate pH) to a final volume of 10 μl. Subsequently, 1 μl of the 1 M orthosilicic acid solution was added and samples were incubated for 5 min at ambient temperature. Samples were centrifuged for 5 min at 14000*g* and pellets were washed three times with H_2O to remove free silicic acid and phosphate. Washed pellets were resuspended in 10 μl of 1 M NaOH and silica was dissolved by incubation at 95°C for 30 min. Silicium concentrations were determined in these solutions by the β-silicomolybdate method (*19*).
15. Purification of silaffin-1A. HF extract from *C. fusiformis* cell walls was prepared as described (*12*) and fractionated on a size-exclusion column (Superdex-Peptide HR-10/30, Amersham Pharmacia Biotech). Chromatography was performed in buffer A [250 mM NaCl, 20 mM tris-HCl (pH 7.5)] at a flow rate of 250 μl/min. Eluting material was recorded at 226 nm and fractions were analyzed by Tricine–SDS-PAGE (*13*) and Coomassie blue staining. Fractions containing pure silaffin-1A were pooled, dialyzed against H_2O, lyophylized, and dissolved in H_2O to a final protein concentration of 10 to 30 μmol/ml.
16. N. Kröger, R. Deutzmann, M. Sumper, data not shown.
17. N. Kröger, C. Bergsdorf, M. Sumper, *Eur. J. Biochem.* **239**, 259 (1996).
18. E. G. Vrieling, W. W. C. Gieskes, T. P. M. Beelen, *J. Phycol.* **35**, 548 (1999).
19. R. K. Iler, *The Chemistry of Silica* (Wiley, New York, 1979).
20. M. L. Chiappino and B. E. Volcani, *Protoplasma* **93**, 205 (1977).
21. M. A. Borowitzka and B. E. Volcani, *J. Phycol.* **14**, 10 (1978).
22. A. M. M. Schmid and D. Schulz, *Protoplasma* **100**, 267 (1979).
23. K. Shimizu, J. Cha, G. Stucky, D. E. Morse, *Proc. Natl. Acad. Sci. U.S.A.* **95**, 6234 (1998).
24. J. Cha *et al.*, *Proc. Natl. Acad. Sci. U.S.A.* **96**, 361 (1999).
25. T. Mitzutani, H. Nagase, N. Fujiwara, H. Ogoshi, *Bull. Chem. Soc. Jpn.* **71**, 2017 (1998).
26. G. M. Lindquist and R. Stratton, *J. Colloid Interface Sci.* **55**, 45 (1976).
27. Protein concentration was determined by the bicinchoninic acid assay as described [P. K. Smith *et al.*, *Anal. Biochem.* **150**, 76 (1985)].
28. Peptide concentration was determined after acid hydrolysis by HPLC analysis of the PTC amino acid derivatives.

29. We thank G. Lehmann and E. Hochmuth for technical assistance; T. Maurer and H. R. Kalbitzer for NMR analysis; and F. Siedler and H. Sarioglou for MS/MS analysis. We are indebted to G. Wanner for field-emission SEM analysis and R. Wetherbee for help with TEM analysis. We greatfully acknowledge W. Tanner for critically reading the manuscript. This work was supported by the Deutsche Forschungsgemeinschaft (SFB 521).

21 July 1999; accepted 30 September 1999

A Possible 20th-Century Slowdown of Southern Ocean Deep Water Formation

Wallace S. Broecker,[1] Stewart Sutherland,[1] Tsung-Hung Peng[2]

Chlorofluorocarbon-11 inventories for the deep Southern Ocean appear to confirm physical oceanographic and geochemical studies in the Southern Ocean, which suggest that no more than 5×10^6 cubic meters per second of ventilated deep water is currently being produced. This result conflicts with conclusions based on the distributions of the carbon-14/carbon ratio and a quasi-conservative property, PO_4^*, in the deep sea, which seem to require an average of about 15×10^6 cubic meters per second of Southern Ocean deep ventilation over about the past 800 years. A major reduction in Southern Ocean deep water production during the 20th century (from high rates during the Little Ice Age) may explain this apparent discordance. If this is true, a seesawing of deep water production between the northern Atlantic and Southern oceans may lie at the heart of the 1500-year ice-rafting cycle.

Circulation changes in the upper ocean have been shown to be an integral part of El Niño cycles, but there has been relatively little discussion concerning the possibility that circulation changes in the deep sea have occurred during the course of the present century. The last well-documented major change in thermohaline circulation occurred in association with the Younger Dryas cold event that ended ~11,500 calendar years ago (*1*). Only at the time of the so-called 8000-years-ago cooling event is there a suggestion of a weakening in the strength of the Atlantic's large-scale circulation during the present interglacial period (*2*). Rather, circulation is often thought of in terms of a smoothly operating Holocene conveyor (*3*). Now, tantalizing evidence suggests that the current rate of deep water formation in the Southern Ocean may be several times smaller than its average over the course of the last ocean mixing cycle (that is, ~800 years).

There is an apparent inconsistency between long-term ventilation rates based on the global distributions of PO_4^* and ^{14}C and those based on observations of the Weddell Sea over the past two decades (*4*). The distribution of PO_4^* [PO_4^*

[1]Lamont-Doherty Earth Observatory of Columbia University, Palisades, NY 10964, USA. [2]Ocean Chemistry Division, Atlantic Oceanographic and Meteorological Laboratory, National Oceanic and Atmospheric Administration, Miami, FL 33149–1026, USA.